

Spatially controllable chemical vapor deposition

Jae-Ouk Choo and Raymond A. Adomaitis¹
*Department of Chemical Engineering
and Institute for Systems Research
University of Maryland
College Park, MD 20742*

Gary W. Rubloff, Laurent Henn-Lecordier, and Yijun Liu²
*Department of Materials Science and Engineering
and Institute for Systems Research
University of Maryland
College Park, MD 20742*

December 2, 2003

Abstract

Most conventional chemical vapor deposition (CVD) systems do not have the spatial actuation and sensing capabilities necessary to control deposition uniformity, or to intentionally induce nonuniform deposition patterns for single-wafer combinatorial CVD experiments. In an effort to address this limitation, a novel CVD reactor system has been developed that can explicitly control the spatial profile of gas-phase chemical composition across the wafer surface. This paper discusses the simulation-based design of a prototype reactor system and the results of preliminary experiments performed to evaluate the performance of the prototype in depositing tungsten films. Initial experimental results demonstrate that it is possible to produce spatially patterned wafers using a CVD process by controlling gas phase reactant composition.

Topical heading: Process Systems Engineering

Keywords: Semiconductor processing; Chemical vapor deposition; Distributed parameter systems; Simulation.

¹Corresponding author. Email: adomaiti@umd.edu

²Current address: ASM International, 3440 East University Drive Phoenix, AZ 85034-7200.

1 Introduction

Chemical Vapor Deposition (CVD) is one of the essential unit operations in semiconductor manufacturing because of its ability to deposit thin smooth films conformally onto submicron-scale features. CVD processes have evolved together with the semiconductor industry, from early bell-jar CVD reactors to the current cold-wall single-wafer reactor (Xia *et al.* 2000). The continuing reduction of device feature size, growing scale of device integration, expanding number of new electronic materials, and increasing substrate (wafer) size motivate development of the new CVD processes necessary to sustain the advancement of microelectronic technology. However, equipment designs are aimed at specific deposition processes and operating conditions (e.g., pressures, chemical species, flows, temperatures) with the design goal of producing process uniformity across large wafers (300 mm dia, resulting in hundreds of semiconductor chips) at the nominal design conditions. Optimizing a design to CVD and other manufacturing equipment for a specific range of design conditions has a number of fundamental shortcomings:

1. Semiconductor manufacturing processes change rapidly in time (e.g., relative to typical petrochemical processes). Because technology improvements must be implemented incrementally to maintain or improve yields in complex, multi-step wafer production sequences, a new generation of process equipment technology may only emerge after several of these improvement steps.
2. Process conditions for optimal material and device quality often do not meet the across-wafer uniformity requirements for manufacturing, forcing a tradeoff between product performance and manufacturing productivity.
3. Fundamental chemical and physical mechanisms for semiconductor processes are often not well known, so that it is difficult to identify *a priori* the best design which balances the demands of product performance and manufacturing uniformity.
4. Experimentation for process optimization is expensive, requiring sets of runs to investigate and characterize complex process behavior.

1.1 Equipment design for uniformity

Current CVD reactor designs typically consist of a cooled-wall reaction (vacuum) chamber in which one to several wafers are processed. Energy needed to drive the deposition reactions is provided by an inductively-heated susceptor or a wafer stage heated by external lamps or internal resistance heating.

Reactant gases enter the reaction chamber through a gas delivery system, flow over the wafer(s), and the residual gas is pumped out through the chamber exhaust port. Because of the importance of spatially uniform (across-wafer) processing capabilities, showerhead designs for gas delivery to the wafer typically incorporate a high density of uniformly spaced small holes in an attempt to distribute gas flow as uniformly as possible across a large diameter wafer. In addition, reactor design components including chamber, wafer position (and rotation), pumping, heating, and gas inlet are commonly structured to achieve high uniformity with cylindrical symmetry about the wafer.

Significant research effort has been directed towards improving growth uniformity of CVD process. Early experimental and simulation-based process equipment research focused on developing an understanding of the important transport and reaction mechanisms of CVD processes and devising optimization methods to aid process parameter selection. For example, Wang *et al.* (1986) used flow visualization techniques to show that heated wafers can disturb gas flow patterns; their experiments suggested lowering operation pressures to reduce the perturbation. Moffat and Jensen (1988) demonstrated the utility of simulation technology for process optimization in the context of a horizontal Si homoepitaxial deposition reactor. Their simulation study examined the relationship between the growth uniformity and tilt angle of the susceptor, giving the optimal setting for this reactor geometry parameter. Another example of rigorous modeling and simulation was performed by Kleijn *et al.* (1989). Their mathematical model was used to show the significance of thermal diffusion and its effect on growth uniformity and gas-phase reactant species distribution.

The evolution of CVD reactor designs also has been motivated by the need to improve growth uniformity. For example, various showerhead designs have been developed to generate uniform gas flow patterns over the wafer surface (Gadgil 1993; Wang *et al.* 1986) or to produce uniform film deposition rates (Kobayashi *et al.* 1997; Kim and Lee 1997). Still more advanced design features are found in the annular, three-zone Texas Instruments showerhead (Moslehi *et al.* 1995) for tungsten and other CVD processes, where individual gas mass flow controllers could be used to set the gas flow rate to each segment.

In some MOCVD processes, the separation of gas precursors is critical because highly reactive gas precursors can cause undesirable gas phase reactions. In an effort to reduce gas phase reactions, Van der Stricht *et al.* (1997) developed a vertical reactor with separate feed ports for each precursor species, and experiments revealed the relationship between the wafer rotation rate and thickness uniformity of GaN and InGaN films. Another example of using separate gas injectors for individual precursors can be found in the horizontal flow MOCVD reactor introduced by Yang *et al.* (1999).

Theodoropoulos *et al.* (2000) described a new MOCVD reactor design of featuring an annular-ring showerhead configuration that allowed the controlled injection of separate precursors. Several annular ring designs were evaluated in this study, and as with Van der Stricht and Yang, Theodoropoulos and co-workers concluded that novel gas delivery designs offered new operational degrees of freedom with which uniformity could be controlled; they also pointed to the importance of simulation tools in selecting optimized operating conditions.

CVD reactor designs have been developed specifically to allow or improve active control of wafer processing conditions during the dynamic processing cycle. For example, work at TI (Moslehi *et al.* 1992) exploited multiple (3 and 4) heating zones radially across the wafer in single-wafer rapid thermal processing to achieve temperature uniformity. This approach has been incorporated into commercial RTP equipment, e.g., from CVC Products, Inc., and from Applied Materials. The SEMATECH testbed RTP system (Stuber *et al.* 1998) and the three-zone RTP system at North Carolina State University (Kiether *et al.* 1994) exploit independent lamp zones for edge-cooling compensation and dynamic uniformity control. Further developments in this area include reduced-model-based real-time control studies of the three-zone NCSU RTP system (Theodoropoulou *et al.* 1999; Christofides 2001) and reduced-model-based order state estimation and optimal control of a horizontal high-pressure CVD system (Banks *et al.* 2002; Kepler *et al.* 2000, 2001).

1.2 The Programmable Reactor concept

The existing design strategy of semiconductor CVD manufacturing equipment faces fundamental barriers limiting the development of next-generation reactor systems; there is a need for a new design paradigm to: (1) decouple fundamental materials and product quality requirements from across-wafer uniformity in manufacturing, so that both may be achieved simultaneously; (2) accelerate materials and process learning and optimization; and (3) develop equipment that is flexible and scalable to succeeding generations of the technology.

As a response to these perceived CVD reactor design shortcomings, this paper presents the development of a novel CVD reactor intended to improve across-wafer 2-dimensional controllability. This new CVD reactor introduces a segmented showerhead design featuring individually controllable gas distribution actuators, a design that reverses the residual gas flow by directing it up through the showerhead, and sampling ports for in-situ gas sampling (Fig. 1). In this paper, we describe the development of this novel design concept by simulation, a sequence of experiments performed using a prototype reactor, and the interpretation of preliminary experimental data by simulation to

demonstrate the validity of the design principles.

We refer to this design as the Programmable CVD Reactor concept because of the potential real-time control of gas phase composition across the wafer surface has for making possible novel operating modes. For example, this reactor design will enable single-wafer combinatorial experiments in which different materials can be created or different process conditions can be tested in a single experiment, producing the library wafer illustrated in Fig. 2. In subsequent deposition runs, the reactor then can be reprogrammed to produce uniform films corresponding to one point on the library wafer without making any hardware adjustments. This mode of operation is made possible by the combination of the flexible design of the Programmable Reactor and model-based interpretation of the sensor and metrology data collected during the processing of the library wafer.

2 Reactor Design Principles

A common feature of all the CVD systems discussed in the previous section having the capability of controlling spatial variations in gas composition leaving the showerhead (e.g., Moslehi *et al.* 1995 and Theodoropoulos *et al.* 2000) is that the actuation capabilities are limited to 1-dimensional control in the radial direction. Furthermore, a characteristic common to these designs is the segment-to-segment interaction produced by the net flow of reactant gas across the wafer to the reactor chamber exhaust. For example, consider the simulation results presented in Fig. 3, where the total gas flow from each of the three injection segments of the showerhead are adjusted to produce a nearly uniform gas velocity field over the wafer radius. If inert gas is injected through the center and outer annular region, and the deposition precursor species are injected through the middle annular injection port, it is easy to see that the net convection across the wafer shifts the region where the precursor plume interacts with the wafer surface downstream relative to the injection point. Therefore, the net flux across the wafer surface, inherent in the annual segmented showerhead designs, reduces the ability to accurately control gas phase composition at the wafer surface.

As an alternative to reactor systems based on the annular segmented showerhead design, the Programmable Reactor system incorporates three new design features to improve the spatial control of gas phase composition. The first is the development of a showerhead design consisting of an assembly of hexagonal showerhead sub-elements (segments) arrayed across the wafer surface. The reactant gas composition and feed rate is controllable within each segment, resulting in true 2-dimensional control of gas composition across the wafer. The spatial resolution with which gas phase composition can be controlled is determined by the size of showerhead segments.

The second new design feature is the recirculation of residual gas up through each segment of the showerhead; exhaust gases mix in a common exhaust volume above the showerhead honeycomb structure (Fig. 1). When the total volumetric flow rate of feed gas to each segment is equal, the effect of this design feature is to create periodic flow fields in the region between the bottom of the showerhead assembly and the wafer surface (Fig. 4). This simulation result was produced using the Fluent CFD package and is based on gas flow rates, compositions, and showerhead segment length scales comparable to the prototype system that was constructed, and which is described later in this paper. In this simulation result it is possible to see that the boundaries of the periodic flow field match the segment wall locations, indicating that there will be no convective flux of reactant species between the segment regions, eliminating the problems generated by drawing exhaust gas across the wafer surface.

The elimination of inter-segment region convective transport will improve the accuracy with which gas composition can be controlled across the wafer surface because across-wafer transport will be governed solely by diffusion. The third new design feature of the Programmable Reactor is the ability to manipulate the showerhead/wafer gap size. Small gap settings will reduce inter-segment diffusion in the gap region leading to deposition of distinct hexagonal patterns; increasing the gap size will spread the pattern, ultimately producing smooth concentration gradients across the wafer surface when reactant gas composition varies from segment-to-segment. An example of the smooth concentration gradients across the wafer surface that can be produced in this manner is shown in the simulation results depicted in Fig. 5, where the across-wafer concentration profile of a particular reactant species is shown for a two-segment reactor design. As with the previous simulation, this simulation result was produced using the Fluent CFD package and is based on gas flow rates, compositions, and length scales comparable to the prototype system.

Because of the reduced effect the gas velocity field has on the gas concentration profile across the wafer surface, the accuracy of simulators used to interpret deposition data will be enhanced, improving the ability to correlate process operating conditions with film properties at all points on the library wafer. Because of the potential for accurately predicting the continuous variation of gas phase concentration across the wafer surface, it may be possible to generate library wafers with continuously graded characteristics across the wafer surface, increasing the information that can be obtained from a single deposition run. The system then can be run with closer showerhead-wafer spacing to produce a finite number of hexagonal patches of material selected from the first library wafer, to provide a more accurate assessment of the process conditions needed to produce the desired

material.

2.1 Prototype construction

To test the feasibility of the Programmable CVD concept, a prototype reactor was designed and constructed by modifying one reaction chamber of an Ulvac-ERA1000 CVD cluster tool (Fig. 6). The Ulvac cluster tool located on the University of Maryland's campus is a commercial CVD system used for selective tungsten (W) deposition. W CVD, used to form vertical interconnects in VLSI and ULSI circuits, represents a relatively mature, but commercially important, manufacturing process (Ireland 1997), and so was chosen for evaluating the engineering design of the programmable reactor. While W CVD deposition mechanisms and reactor systems have been studied extensively (e.g., Arora and Pollard 1991; Kleijn 2000; Kleijn *et al.* 1991; Kleijn and Werner 1993), open process development issues remain. Even in the simplest case of blanket deposition using H_2 and WF_6 , the reactant/reducing gas ratio and WF_6 gas concentration result in two operational degrees of freedom that force a tradeoff between film conformality and deposition rate, where the latter is compounded by reactor design factors that determine where the transition from reaction rate to mass-transfer limited operation takes place.

In its original configuration, the hydrogen reducing gas entered through a quartz showerhead above the wafer; wafer heating was provided by a ring of heating lamps above the showerhead. As part of the Programmable Reactor modifications, substrate heating was used in place of lamp heating, and the quartz showerhead was replaced by the new Programmable Reactor showerhead assembly. The primary component of the assembly is the honeycomb-shaped array of three segments machined from a single block of stainless steel. Each side of the hexagonal segments is $W = 1in$ in length and the overall length of the honeycomb segment structure is $L = 5.67in$. As designed, the three segments cover most of the surface area of the $4in$ wafers used in deposition experiments. The segment length was made as long as physically possible subject to the constraints imposed by clearances necessary to insert the wafer and to prevent obstruction of the exhaust ports in the showerhead chamber.

Each segment is fitted with two $0.25in$ ID feed tubes and one sampling tube (Figs. 7 and 8). The feed and sampling tube vertical positions can be adjusted when the reactor is not operating. The sampling tube of each segment can be used to transport a small amount of gas to a real time in-situ sensor, such as a mass spectrometer. From the residual gas analysis of each segment, approximate film thickness and the composition of film deposited on each area corresponding to each segment

can be determined (Gougousi *et al.* 2000).

Individual mass flow controllers with a range of 0 – 100sccm were used to control the total flow of H₂, Ar, and WF₆ to the showerhead; a network of needle valves was used to split these gas flows to each showerhead segment. Showerhead/wafer spacing is controlled with the linear motion device shown in Fig. 7. In addition to controlling inter-segment region diffusion, the linear motion device is needed to raise the honeycomb structure sufficiently to allow the cluster tool's robot arm to insert and withdraw the wafer from the reactor chamber.

3 Modeling and Simulation

Because of the Programmable CVD reactor's reverse-flow design, reactants in the gas mixture in the common exhaust volume can diffuse back into the segments. Therefore, to sustain the pre-specified gas compositions at the bottom of each segment, the back diffusion through the segment should be suppressed below an acceptable level by the convective upward flux contribution to species transport in each segment. A steady-state 1-dimensional segment model (for each segment) combined with a well-mixed common exhaust volume model and a model of inter-segment transport in the gap region between the wafer and showerhead segments for nonzero gap size is developed in this section. The geometry of a single segment, together with the notation used in the model development, is shown in Fig. 9.

This model was used to determine feed gas flows to the individual segments and to interpret preliminary experimental observations. In particular, the simulator was used to assess the ability of the segmented structure to maintain significant segment-to-segment gas composition differences near the wafer surface when the reactor was operated under the extreme condition of supplying pure Ar to segment 1, pure WF₆ to segment 2, and pure H₂ to segment 3.

3.1 Exhaust volume

As the first step in developing a model of reactant transport through each segment (Fig. 9) and between each segment in the wafer/showerhead gap region, the mole fraction of each species denoted as

$$x_i^k(z) \quad : \quad i = \text{H}_2, \text{WF}_6, \text{Ar} \quad k=1,2,3 \quad 0 \leq z \leq L$$

where the the subscript i refers to the gas species and k the segment number.

For this simulation study, the common exhaust volume was treated as perfectly mixed. Because of the relatively low depletion rate of the deposition reaction under the chosen operating conditions

(this assumption will be validated at the end of this paper), the exhaust volume composition x_i^{exh} was computed simply as the average of the feed compositions to each segment.

3.2 Inter-segment diffusion

The rate of across-wafer chemical species transport is determined by the gap size h between the honeycomb showerhead structure and wafer surface and the composition differences between the reactant gases at the bottom of each segment and the chamber itself. A simplified model of inter-segment transport in this gap region can be derived for the experiment where pure gases are fed to each segment. For example, the flux of Ar from segment region 1 (where it is the primary feed gas) to segment 3 (where H₂ is the primary feed) can be written as

$$N_{Ar}^{1-3} = CD_{Ar,H_2} f_d \frac{x_{Ar}^3(0) - x_{Ar}^1(0)}{2W \cos(\pi/6)} \quad (1)$$

where the length scale of the finite-difference approximation to the composition gradient is the distance from the center of one hexagonal segment to the center of the adjacent segment. The flux correction factor f_d will be estimated from experimental data later in this paper. Because the chamber gas phase composition could not be measured in the experiments discussed in this paper and because of the likelihood of WF₆ depletion due to heated reactor components, transport between segment regions and the outer chamber are not included in this simulation study. The binary diffusion coefficients D_{ij} are estimated by the Chapman-Enskog kinetic theory and Neufield method (Kleijn and Werner 1993; Reid *et al.* 1987). C is the total gas concentration. A complete summary of the parameters and variables used is presented in Table 2 at the end of this paper.

These values of inter-segment species flux then are used as the initial value of the intra-segment flux terms:

$$N_i^k(z) = \frac{hW}{A_s} \sum_{n=1}^3 N_i^{k-n} + F_i^k(z)$$

where F_i^k is a function accounting for the change in flux due to fresh feed of species i from the segment feed tubes and is defined by

$$\begin{aligned} F_i^k &= 0 & z < z_f \\ F_i^k &= Q_i^k \rho_i / (M_i (A_s - A_f)) & z \geq z_f \end{aligned}$$

where Q_i^k is the volumetric flowrate of gas species i to segment k .

3.3 Intra-segment transport

Neglecting any effect of pressure and forced diffusion, the multicomponent gas species transport can be expressed by the Maxwell-Stefan equation

$$\nabla x_i^k = \sum_{j=1}^n \frac{1}{CD_{ij}} (x_i^k N_j^k - x_j^k N_i^k) + \sum_{j=1}^n \frac{x_i^k x_j^k}{D_{ij}} \left(\frac{D_j^T}{\rho_j} - \frac{D_i^T}{\rho_i} \right) \nabla \ln T \quad 0 < z < L$$

subject to boundary conditions

$$x_i^k(L) = x_i^{exh}. \quad (2)$$

The gas temperature profile along the segment length z is needed to compute the contribution of thermal diffusion; observation of the W film deposited on the segment structure after a number of experimental runs indicates that there is significant gas and segment heating along the bottom-most third of the honeycomb segments. Given this observation, the gas temperature was approximated as a linear interpolation between the wafer (maintained at 350°C) and the ambient temperature (30°C) over the bottom third of the segment, and was set as the ambient temperature for the remainder of the segment.

The flux due to ordinary diffusion can be defined as

$$\bar{N}_i^k = N_i^k + \frac{D_i^T}{M_i} \nabla \ln T$$

giving the simplified form of the Maxwell-Stefan equation

$$\nabla x_i^k = \sum_{j=1}^n \frac{1}{CD_{ij}} (x_i^k \bar{N}_j^k - x_j^k \bar{N}_i^k) \quad (3)$$

subject to boundary conditions (2). The D_i^T are the multicomponent thermal diffusion coefficients computed using the correlations given in Kleijn and Werner (1993).

4 Simulation Results

The nine inter-segment flux equations (1) are solved simultaneously with the nine collocation-discretized Maxwell-Stefan equations (3) subject to boundary conditions (2) using a Newton-Raphson method to obtain the gas composition profiles as a function of position within each segment. 20 collocation points located at the zeros of 19th-degree Chebyshev polynomial, plus the interval endpoints, were used to define the discretization arrays (Adomaitis 2002).

Because the modeling equations for each segment are identical in structure and vary only in terms of parameter values, an object-oriented approach was taken to setting up the simulator: a

segment model class (in MATLAB) was derived from an abstract class defining the general structure of a nonlinear algebraic equation model. Methods for the nonlinear equation model class included a Newton-Raphson based equation solver, which is inherited by the segment model class. Because each segment model is an instance of the latter class, this approach is an efficient method for setting up models of this form, and is readily extensible to Programmable Reactor models with many more segment elements. More details on the computational approach will be given in a later paper.

Representative results of this solution procedure are shown in Fig. 10. In this Figure, the wafer surface is located at $z = 0$ (the left axis limit) and the segment top is to the right; the vertical line represents the location z_f of the bottom of the feed tube bundle inside each segment. Two sets of simulations were performed to assess the effect total gas flow to each segment has on the composition profiles, and the results are discussed below. In each case, the gap size h was set to 0. Simulations to evaluate the effect of gap size h will be performed later in this paper to interpret some of the experimental findings.

4.1 Low-flow results

Simulator predictions for the gas composition profiles of Segments 1 to 3 (ordered from the top plot) for a gas feed flow of $Q = 2.5\text{scm}$ to each segment are shown in the left column of plots in Fig. 10. The composition in each segment as $z \rightarrow L$ approaches the composition of the gas in the common, well-mixed exhaust chamber. As the profiles are followed down the segments, the feed gas species of each segment becomes the primary component. However, because of the relatively low flow, significant back-diffusion of the other components occurs resulting in a significant fraction of each species being found near the bottom of each segment - this is particularly true in Segment 3 because of the larger fraction of H_2 and the larger values of binary diffusion coefficients when H_2 is one of the species. It is also interesting to observe the effect thermal diffusion has in this simulation - in each case, the region near the wafer is enriched in H_2 relative to the heavier species due to thermal diffusion. Thus, because of the large negative effect ordinary and thermal diffusion have on the ability to control gas composition near the wafer surface, it is possible to conclude that higher feed flow rates should be used.

4.2 High-flow results

Increasing the gas flowrate to 50scm in each segment has a dramatic effect on the gas composition profiles in each segment. As can be seen in the right column plots of Fig. 10, the feed species to

each segment becomes the dominant gas phase species near the wafer surface. Thermal diffusion effects still can be observed, but have a much lower impact on the composition profiles. Under these operating conditions, the effect of changing the gap size on gas composition near the wafer surface should be more pronounced, and so initial experiments were conducted at these conditions. It should be noted that while the WF_6 concentration at the bottom of Segments 1 and 3 is very small, it is nontrivial and so can (and does) result in film deposition under these segments.

5 Prototype Experimental Tests

Initial experiments were performed using the three zone prototype to validate two basic Programmable Reactor design concepts: (1) that the reverse-flow showerhead design could maintain significant segment-to-segment gas-phase compositional differences near the wafer surface, and (2) that spatially patterned wafers could be produced by this reactor design and that some of the characteristics of the pattern can be controlled by manipulating the showerhead/wafer gap. Typical operating conditions for the first experiments consisted of a 0.5 torr chamber pressure, a wafer temperature of 350°C , and 10-20 minute deposition times. The film thickness in the region below each segment was determined by sheet resistance measurements using a four-point probe.

5.1 Segment-to-segment gas composition differences

In the set of experiments discussed in this paper, pure Ar was fed to Segment 1 at a flowrate of 50sccm ; 50sccm of WF_6 was fed to segment 2, and 50sccm of H_2 was fed to segment 3. Sheet resistance measurements were made at seven points on the wafer surface in each segment region; the data are interpolated and plotted in Fig. 11. Simulator predictions for these conditions indicate that the gas composition at the wafer surface is mainly the segment feed species, with a small amount of WF_6 present at the bottom of segments even when $h = 0$ (Fig. 10). While W deposition should take place directly under Segment 2 (where pure WF_6 is fed) due to the Si reduction mechanism, it is interesting to note that some W deposition takes place under the remaining two segments. Further experimental data and simulator predictions will validate that the WF_6 responsible for deposition in segments 1 and 3 is transported to this region through a combination in back-diffusion and inter-segment diffusion.

5.2 Control of pattern resolution

In all cases where the showerhead/wafer spacing was small (e.g., $h = 1\text{mm}$), distinct hexagonal film patterns were produced (Fig. 12). As the gap is increased, the contribution of back-diffusion down the segments from the common exhaust remains essentially constant while inter-segment diffusion in the gap region increases. Photographs of wafers processed for three different gap values are shown in Fig. 12 demonstrating that the pattern becomes more diffused with increasing gap size. This decrease in the sharpness of the deposition pattern provides visual evidence for the effectiveness of using gap size to control inter-segment diffusion of reactant species across the wafer surface.

Across-wafer diffusion of WF_6 from Segment 2 to the Ar- and H_2 -fed segments should result in a negative film thickness gradient along lines drawn through the latter two segments in the direction away from Segment 2 (as seen in the two lines marked in Fig. 11). This is clearly evident in the linear interpolation plots presented in Fig. 13, where the film thickness along these two “cuts” in Segments 1 and 3 is plotted for three different values of gap size. Furthermore, we observe the overall thickening of the film in these two segments as the gap increases, a phenomenon attributable to the increased WF_6 concentration resulting from increasing inter-segment diffusion as the gap is increased. Likewise, extrapolating the growth rates of Segments 1 and 3 to $h = 0$ (which is an undesirable experiment to perform) shows positive growth rates in each segment for zero gap, indicating the contribution of intra-segment back-diffusion of WF_6 to the growth rate in each of these segments. It is interesting to note the greater slope of the deposition rate line (as a function of h) in Segment 1 relative to Segment 3; this may be attributable to the smaller binary diffusion coefficient in an Ar- WF_6 mixture compared to a H_2 - WF_6 mixture.

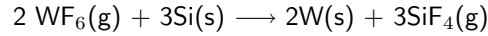
Finally, error bars indicating the standard deviation of all seven sheet resistance measurements per segment are plotted; the slightly increasing trend with gap size may indicate additional effects of inter-segment and chamber-segment diffusion on film thickness variation within each segment region as the gap increases. For increasing values of very large values of h (e.g., $< 10\text{mm}$), the variability should begin to decrease with h due to the dominance of across-wafer diffusion under these operating conditions.

6 Simulation-Based Interpretation of Film Deposition Results

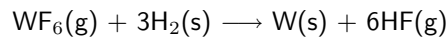
Thin films of tungsten can be deposited in either a selective or blanket tungsten deposition mode. The gas phase reactions associated with these deposition processes are negligible due to low reactor

pressure during the process operation (Arora and Pollard 1991; Kleijn *et al.* 1991), therefore, the deposition rate is determined only by surface reaction and chemical species transport rates in the gas/wafer surface interface and through the deposited film itself.

The overall reaction of tungsten deposition by hydrogen reduction on a silicon wafer substrate begins with surface reactions by Si reduction during the film nucleation step; the reaction is



in the range of deposition temperature used in our experiments (Leusink *et al.* 1992). Numerous studies have focused on the extent to which this reaction takes place and when the transition to the H_2 reduction process



occurs. Most studies conclude the Si reduction step is self limiting and typically accounts for 10-200nm of W film thickness at the Si substrate/W film interface (Groenen *et al.* 1994). However, Joshi *et al.* (1992) presented a counterexample study in which non-self-limited growth was observed using two different CVD systems, resulting in relatively thick W films. A mechanism for this deposition process was proposed whereby Si out-diffused from the substrate through the deposited W film and reacted with WF_6 on the film surface; this process was found to be promoted by oxygen impurities in the W film. The expression for the overall deposition rate was determined to be the product

$$\frac{ds_w}{dt} = R_k R_d$$

(after eq. A5 in Joshi *et al.* 1992) where the rate of change of film thickness s_w is the product of the reaction rate of Si with WF_6 at the film's top surface

$$R_k = \frac{K_0}{N_{\text{Si}}} [Cx_{\text{WF}_6}]^n e^{-E_a/RT} \quad (4)$$

and the rate at which Si atoms diffuse from the substrate through the W layer to the film surface:

$$R_d = \frac{C_0}{1 + K_0 s_w [Cx_{\text{WF}_6}]^n e^{-E_a/RT} / D}.$$

See Joshi *et al.* (1992) for a complete description of the parameters in these rate expressions. For short deposition times or thin films ($s_w \rightarrow 0$) produced by low deposition temperature or low WF_6 concentration, the term describing the rate of diffusion becomes a constant and the deposition rate is determined only by the surface reaction rate R_k (in the absence of gas-phase transport limitations).

6.1 Simulated vs. measured deposition rates

Simulation of the deposition process in Segments 1 and 3 can be used as an indirect method to quantify the rate of inter-segment transport in the wafer/showerhead gap region. This will be carried out by estimating the parameter f_d in (1) and the reaction rate coefficients K^k in the simplified rate expression for growth of very thin films by Si reduction in segments $k = 1, 3$:

$$\frac{ds_w^k}{dt} = K^k [x_{WF_6}^k(0)]^{0.5}.$$

Simulations were performed using the three-segment reactor model for gap values of $h = 1, 3, 5\text{mm}$ and a fixed value of f_d to obtain the values of $x_{WF_6}^k(0)$ for segments $k = 1, 3$. A least-squares fit of the rate coefficients K^k to the experimentally measured rate data then was performed; the optimal value of f_d was determined by minimizing the error in this regression. The parameter values obtained using this estimation method are:

$$f_d = 0.2 \quad K^1 = 1.92 \text{ nm/min} \quad K^3 = 0.36 \text{ nm/min}$$

Simulator predictions of growth rates as a function of h are compared to experimental data in Fig. 14.

That a good fit is obtained for the rate exponent of 0.5 (recommended by Joshi *et al.* 1992) is significant because an accurate rate description for rates linear in WF_6 concentration and that pass through $ds_w/dt = 0$ for $x_{WF_6} = 0$ could not be found for these data. The different values of K^k determined for each segment can be attributed to the different wafer surface temperatures in each segment due to gas composition differences (Chang *et al.* 2001) or film surface condition differences resulting from the H_2/Ar composition differences.

The resulting simulator predictions are consistent, qualitatively as well as quantitatively, with the observed reactor behavior, indicating the importance of intra-segment back-diffusion and inter-segment diffusion across the wafer surface in governing the observed deposition rates, and how these processes can be controlled by adjusting the gap size and feed gas flow rate in this reactor design. Finally, in Table 1, the magnitude of gas species fluxes due to bulk flow up the segment, the diffusion processes, and the deposition rate are compared to justify the original assumption that the deposition rate is low compared and could be neglected in the original derivation of the reactor segment model.

7 Conclusions

A new approach to designing spatially controllable chemical vapor deposition reactors was presented in this paper. The primary design innovation of this CVD system was the introduction of a segmented,

<i>Flux</i>	<i>Value, mol/(m²s)</i>
convective (F_i^k)	O(10 ⁻²)
intra- and inter-segment (N_i^{j-k})	O(10 ⁻⁵)
deposition rate	O(10 ⁻⁷)

Table 1: *A comparison of fluxes predicted by the reactor simulator.*

reverse-flow gas delivery (showerhead) assembly. A three segment prototype reactor was constructed to prove the validity of the design concept and provide engineering data for simulator development. Preliminary experimental testing demonstrated the validity of the design by depositing spatially patterned films using the reactor’s ability to control across wafer gas composition. Simulation studies were performed to interpret experimental data and to estimate gas phase composition at the wafer surface.

This approach to thin-film manufacturing control opens the door to a new generation of CVD reactor design, allowing single-wafer combinatorial studies and precise across-wafer uniformity control in a single reactor design. The modular nature of the showerhead segments offers the possibility of developing CVD reactors for very large substrates. To reach these goals, a new reactor is under construction that includes a more precisely controllable reactant gas delivery system, a cleaner reaction chamber environment, and better access to the wafer while the deposition process is taking place. It is anticipated that the additional instrumentation in the next prototype will allow a demonstration of the programmability capabilities envisioned for this system. Research in improving the manufacturability of the showerhead segment modules, particularly integrating feed gas flow control into each segment, also is in progress.

8 Acknowledgments

The authors acknowledge the support of the National Science Foundation through grant CTS-0085632 for construction of the prototype and simulation work, the continued support of NSF through CTS-0219200, and National Institute of Standards and Technology for fabricating several showerhead components.

<i>Symbol</i>	<i>Units (and Value)</i>	<i>Description</i>
A_f	$9.5 \times 10^{-5} \text{ m}^2$	feed + sample tube cross section area
A_s	0.0016 m^2	segment cross section area
C	mol/m^3	total concentration
D	m^2/s	diffusivity of Si in W
D_{ij}	m^2/s	binary diffusion coefficient
D_i^T	$\text{kg}/(\text{m}\text{s})$	thermal diffusion coefficient
f_d		inter-segment transport correction factor
h	m	wafer/segment-bottom gap size
K^k	nm/min	W deposition rate coefficient
L	0.144 m	segment length
M_i	kg/mol	species i molecular weight
N_i^k	$\text{mol}/(\text{m}^2\text{s})$	species i segment k total molar flux
\bar{N}_i^k	$\text{mol}/(\text{m}^2\text{s})$	species i segment k ordinary diffusion flux
Q_i^k	m^3/s	segment k feed flow rate of species i
s_w	m	W film thickness
t	s	time
T	K	segment gas temperature
W	0.025 m	segment side length
x_i^k		species i segment k mole fraction
z	m	1D segment coordinate
z_f	0.0508 m	feed tube outlet location
ρ_i	kg/m^3	pure species gas density

Table 2: *List of variables and parameters*

9 References

- Adomaitis, R. A. (2002) Objects for MWR, *Comp. & Chem. Engng* **26** 7-8, 981-998.
- Arora, R. and R. Pollard, (1991) A mathematical model for chemical vapor deposition process influenced by surface reaction kinetics: application to low-pressure deposition of tungsten, *J. Electrochem. Soc.* **38** (5) 1523.
- Banks, H. T., S. C. Beeler, G. M. Kepler, and H. T. Tran (2002) Reduced order modeling and control of thin film growth in an HPCVD reactor, *SIAM J. Appl. Math.* **62** 1251-1280.
- Chang, H. -Y., R. A. Adomaitis, J. N. Kidder, Jr., and G. W. Rubloff (2001) Influence of gas composition on wafer temperature in a tungsten chemical vapor deposition reactor: Experimental measurements, model development, and parameter estimation, *J. Vac. Sci. and Tech.,B* **19** 230-238.
- Christofides, P. D. (2001) *Nonlinear and Robust Control of PDE Systems: Methods and Applications to Transport-Reaction Processes*, Birkhauser Pub. Co.
- Gadgil, P. N., Optimization of a stagnation point flow reactor design for metalorganic chemical vapor deposition by flow visualization (1993) *J. Crystal Growth* **134** 302-312.
- Gougousi, T., Y. Xu, J.N. Kidder, Jr., G. W. Rubloff, and C. R. Tilford (2000) Process diagnostics and thickness metrology for the chemical vapor deposition of W from H₂/WF₆ using in-situ mass-spectrometry, *J. Vac. Sci. Technol. B* **18**, 1352-1363
- Groenen, P. A. C., J. G. A. Holscher, and H. H. Brongersma, (1994) Mechanism of the reaction of WF₆ and Si, *Applied Surface Sci* **78**, 123-132.
- Ireland, P. J., (1997) High aspect ratio contacts: A review of the current tungsten plug process, *Thin Solid Films* **304**, 1-12.
- Joshi, R. V., V. Prasad, M. L. Yu, and G. Scilla, (1992) Non-self-limiting nature of silicon reduction of WF₆ in cold wall systems, *J. Appl. Phys.* **71** (3) 1428-1441.
- Kepler, G. M., H. T. Tran, and H. T. Banks (2000) Reduced order model compensator control of species transport in a CVD reactor, *Optim. Contr. Appl. Meth.* **21** 143-160.
- Kepler, G. M., H. T. Tran, and H. T. Banks (2001) Compensator control for chemical vapor deposition film growth using reduced-order design models, *IEEE Tran. Semicond. Manuf.* **14** 231-241.
- Kiether, W. J., M. J. Fordham, S. Yu, A. J. S. Neto, K. A. Conrad, J. Hauser, F. Y. Sorrell, and J. J. Wortman (1994) Three-Zone Rapid Thermal Processor System. Proc. 2nd Int. RTP Conf., 96-101.
- Kim B. N. and H. H. Lee, Numerical simulation of metalorganic chemical vapor deposition of copper in a single-wafer reactor (1997) *J. Electrochem.Soc.* **144** 1765-1773.
- Kleijn, C. R., (2000) Computational modeling of transport phenomena and detailed chemistry in chemical vapor deposition - a benchmark solution, *Thin Solid Films* **365**, 294-306.
- Kleijn, C. R., C. J. Hoogendoorn, A. Hasper, J. Holleman and J. Middelhoek, (1991) Transport phenomena in tungsten LPCVD in a single-wafer reactor, *J. Electrochem. Soc.* **138**, 509-517.
- Kleijn, C. R., Th. H. van der Meer, and C. J. Hoogendoorn, (1989) A mathematical model for LPCVD in a single wafer reactor, *J. Electrochem. Soc.* **136**, 3423-3433.
- Kleijn C. R. and C. Werner, (1993) *Modeling of chemical vapor deposition of tungsten films*, Basel; Boston: Birkhauser Verlag.
- Kobayashi, A., A. Sekiguchi, K. Ikeda, O. Okada, N. Hosokawa, Y. Tsuchiya, and K. Ueno, The deposition rate for Cu CVD. (1997) In *Advanced Metalization and Interconnect Systems for ULSI Applications*, ed. by R. Havemann, J. Schmitz, H. Komiyama, and K. Tsubouchi, Mater. Res. Soc. Pittsburgh, PA, 177-183.

- Leusink, G. J., C. R. Kleijn, T. G. M. Oosterlaken, C. A. M. Janssen, and S. Radelaar, (1992) Growth kinetics and inhibition of growth of chemical vapor deposited thin tungsten films on silicon from tungsten hexafluoride, *J. Appl. Phys.* **72** (2) 490-498.
- Moffat, H. K. and K. F. Jensen, (1988) Three-dimensional flow effects in silicon CVD in horizontal reactor, *J. Electrochem. Soc.* **135**, 459-471.
- Moslehi, M. M., C. J. Davis, and A. Bowling, *TI Technical Journal*, Sept-Oct 1992, 44-64.
- Moslehi, M. M, C. J. Davis, and R. T. Matthews, (1995) Programmable multizone gas injector for single-wafer semiconductor processing equipment, United State Patent 5,453,124.
- Reid, R. C., J. M. Praunitz and B. E. Poling, (1987) *The properties of gases and liquids* (4th edition), New York, McGraw-Hill.
- Stuber, J. D., I. Trachtenburg, and T. F. Edgar, Design and modeling of rapid thermal processing systems (1998) *IEEE Trans. Semicond. Manuf.* **11** 442-457.
- Theodoropoulos, C., T. J. Mountziaris, H. K. Moffat and J. Han, (2000) Design of gas inlets for the growth of gallium nitride by metalorganic vapor phase epitaxy, *J. Crystal Growth* **217**, 65-81.
- Theodoropoulou, A., E. Zafiriou, and R. A. Adomaitis (1999) Inverse model based real-time control for temperature uniformity of RTCVD, *IEEE Trans. Semicond. Manuf.* **12**, 87-101.
- van der Stricht, W., I. Moerman, P. Demeester, J. A. Crawley and E. J. Thrush, (1997) Study of GaN and InGaN films grown by metalorganic chemical vapor deposition, *J. Crystal Growth* **170**, 344-348.
- Wang, C. A., S. H. Gorves, S. C. Palmateer, D. W. Weyburne, and R. A. Brown, (1986) Flow visualization studies of OMVPE reactor designs *J. Crystal Growth* **77** 136-147.
- Xia, L., P. W. Lee, M. Chang, I. Latchford, P. K. Narwankar, R. Urdahl, (2000) Chapter 11. Chemical Vapor Deposition, *Handbook of Semiconductor Manufacturing Technology*, Yoshi Nishi, Robert Doering, ed., New York: Marcel Dekker.
- Yang, C., C. Huang, G. Chi and M. Wu, (1998) Growth and characterization of GaN by atmosphere pressure metalorganic chemical-vapor deposition with a novel separate-flow reactor, *J. Crystal Growth* **200** 39-44.

Figure 1: *An illustration of the Programmable CVD Reactor three-zone prototype showing the segmented showerhead structure and segment feed lines.*

Figure 2: *A rapid process prototyping approach to new materials and process development. The spatial patterning capabilities of the Programmable CVD Reactor can be used to produce a “library” wafer (left) containing regions of distinct material properties; the reactor system then can be reprogrammed to deposit spatially uniform films of the chosen property (right).*

Figure 3: *Gas concentration field computed for a segmented showerhead design illustrating the mismatch between gas injector location and the resulting gas concentration profile over the wafer surface in a non-reverse flow design.*

Figure 4: *Periodic flow patterns generated by the reverse flow showerhead design.*

Figure 5: *Simulation of gas concentration profile over the wafer surface by a two-zone reverse flow design; note smooth concentration gradient over the wafer surface.*

Figure 6: *The two-chamber Ulvac W CVD cluster tool modified to accommodate the prototype showerhead assembly.*

Figure 7: *Schematic diagram showing a vertical cross-section of the Programmable CVD reactor.*

Figure 8: *The prototype showerhead mounted on one of the Ulvac reactor chambers.*

Figure 9: *Details of a single showerhead segment.*

Figure 10: *Gas composition profiles in each segment for two different gas flow rates for the Ar fed segment (top), WF_6 fed segment (middle), and H_2 fed segment (bottom); the vertical line marks the feed tube bundle outlet location.*

Figure 11: *Film thickness measurements for a representative experiment determined by sheet resistance measurements. Seven measurements were made in each segment region.*

Figure 12: *Deposition patterns produced using three different values for the showerhead/wafer spacing. In these experiments pure Ar, WF_6 , and H_2 were fed to the individual segments.*

Figure 13: *Film thickness measurements for three showerhead/wafer spacing values showing how film thickness shrinks in the Ar and H_2 fed segments with distance from the WF_6 segment (left) and how overall film thickness increases in each segment region as the spacing is increased (right)*

Figure 14: *Simulated predictions of the W deposition rate by Si reduction in the Ar and H_2 fed segments compared to experimental measurements.*

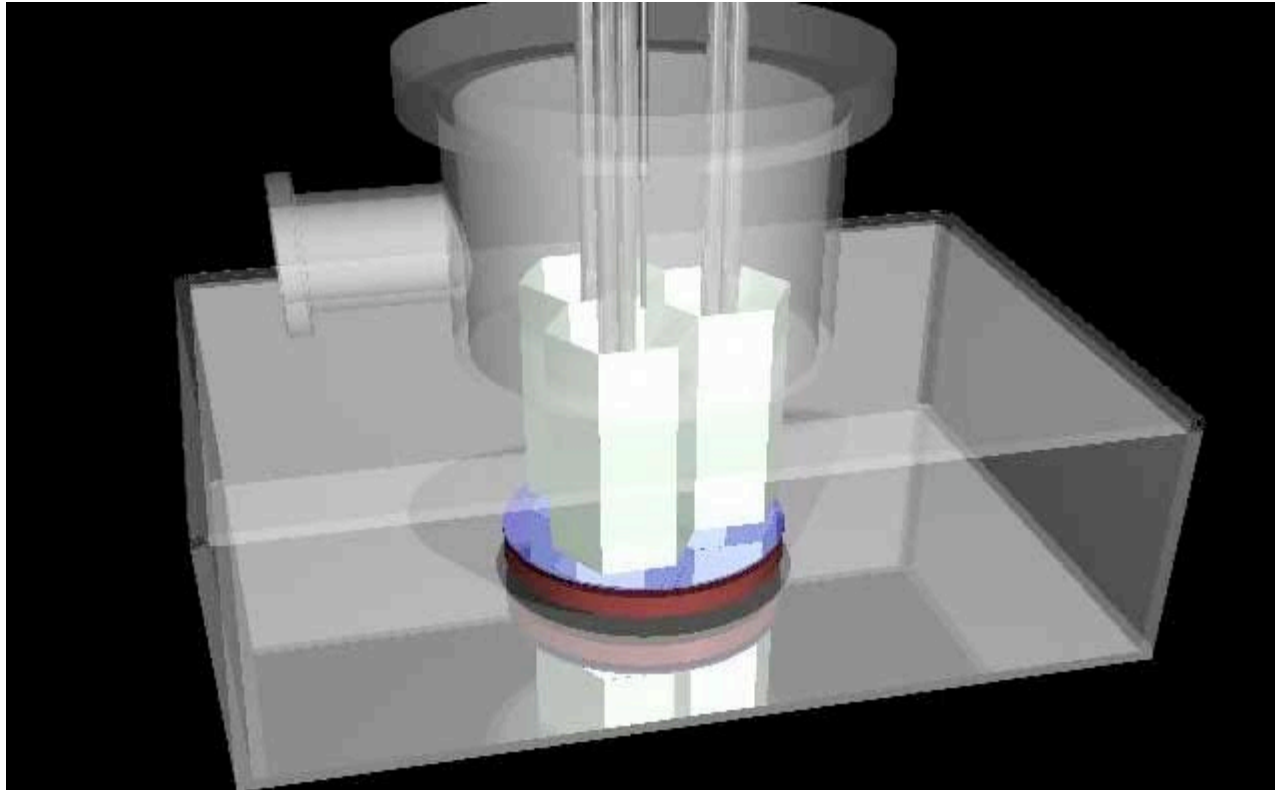
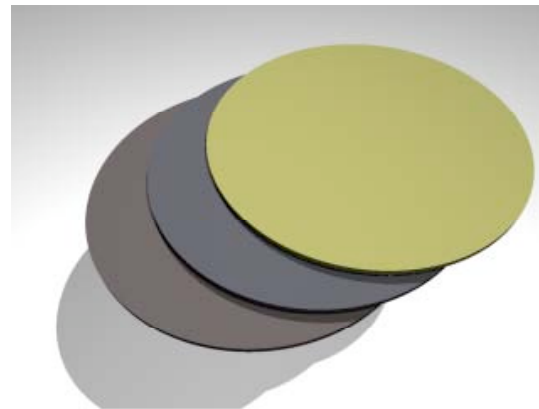
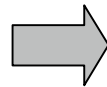


Figure 1



**Library wafer:
programmed nonuniformity**



**Uniform deposition
at specified conditions**

Figure 2

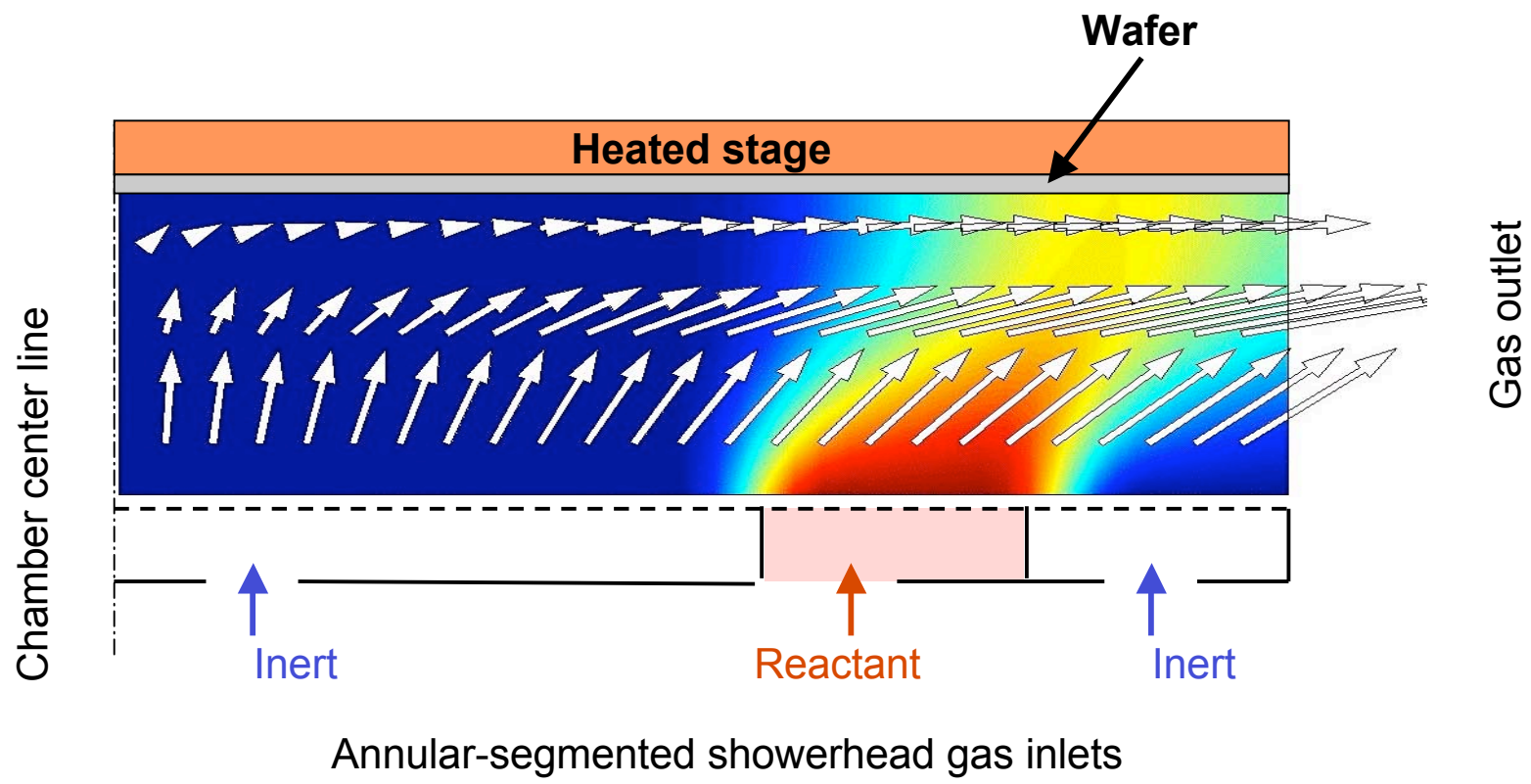


Figure 3

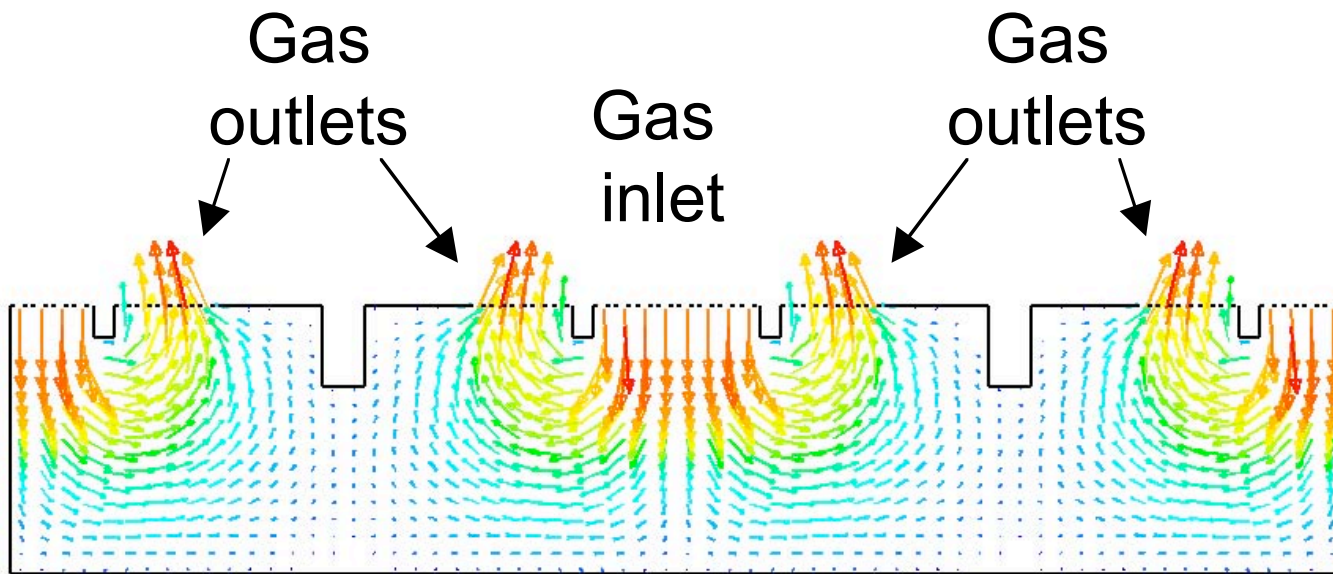
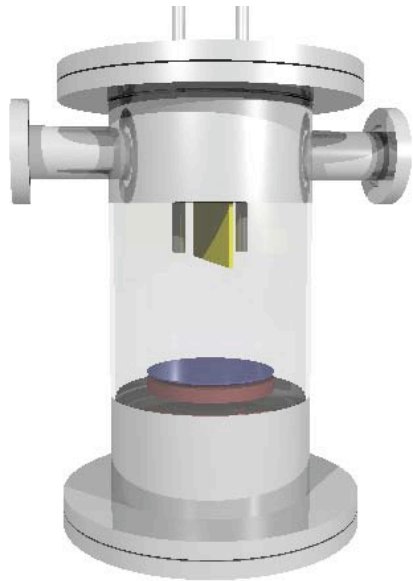
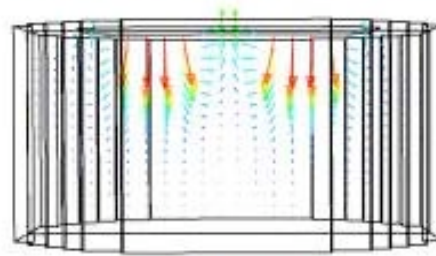


Figure 4



2 feed/exhaust segments



wafer plane

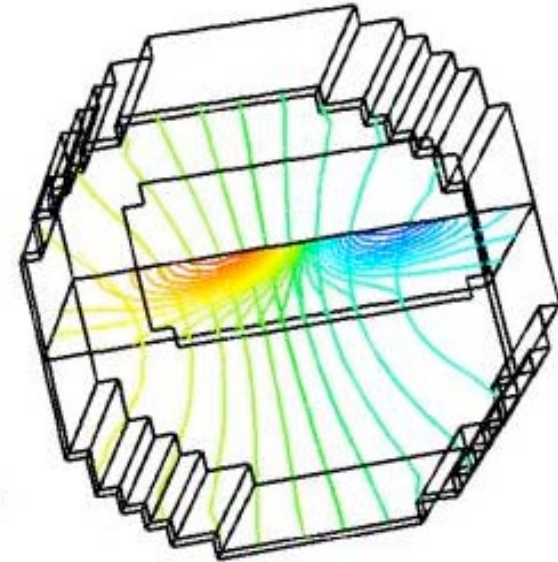


Figure 5



Figure 6

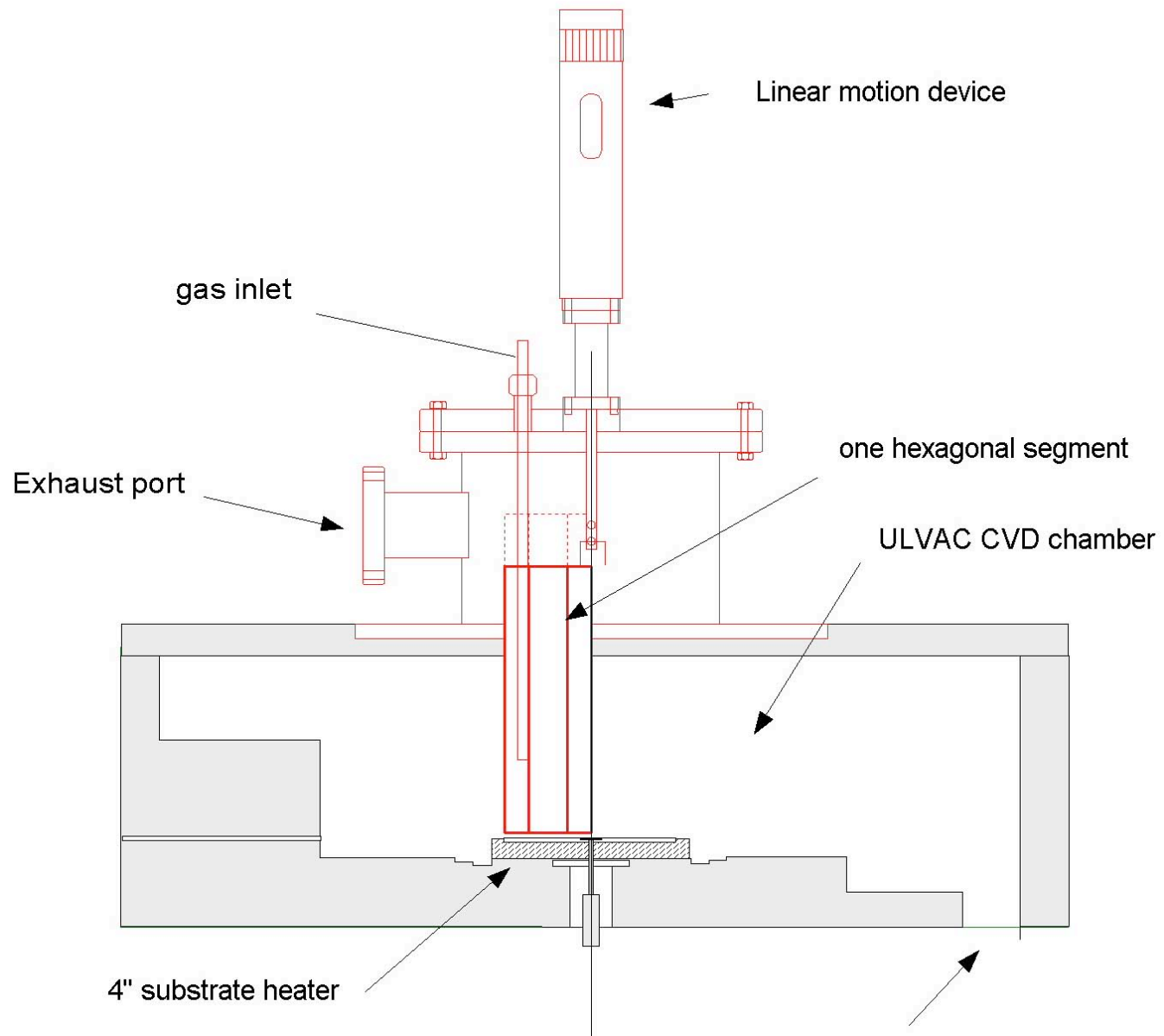


Figure 7

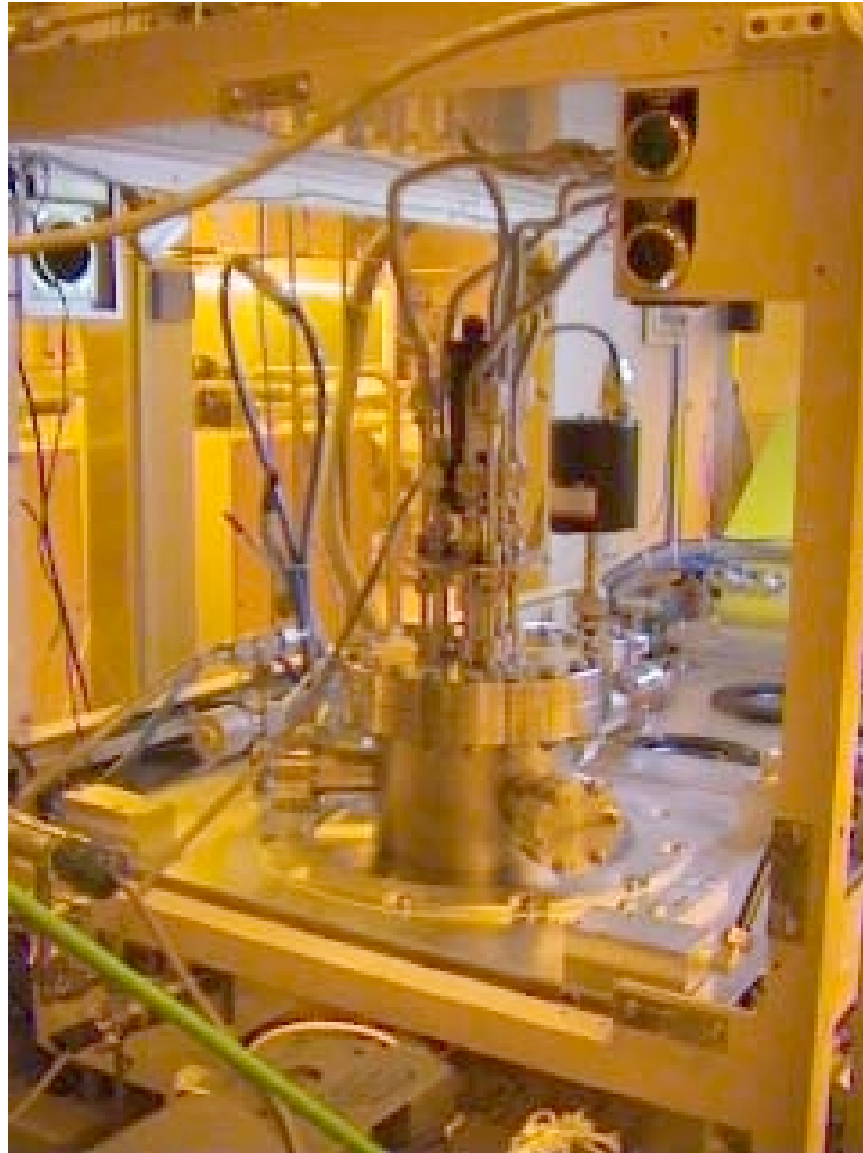


Figure 8

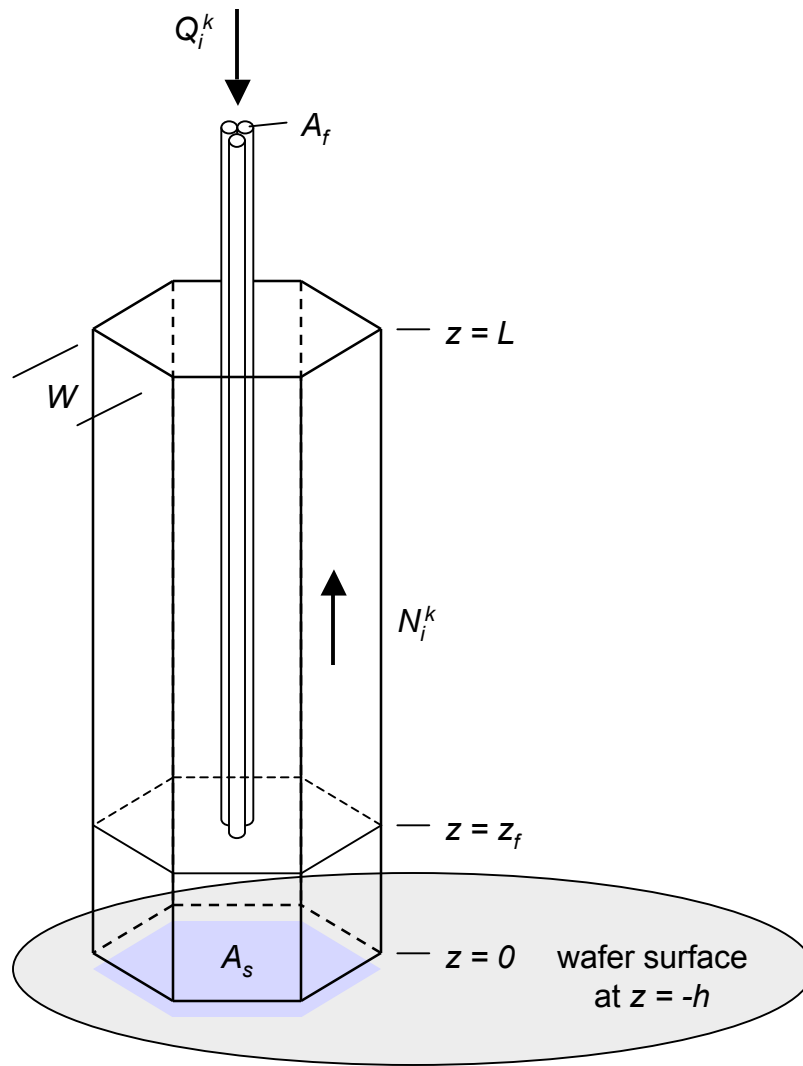


Figure 9

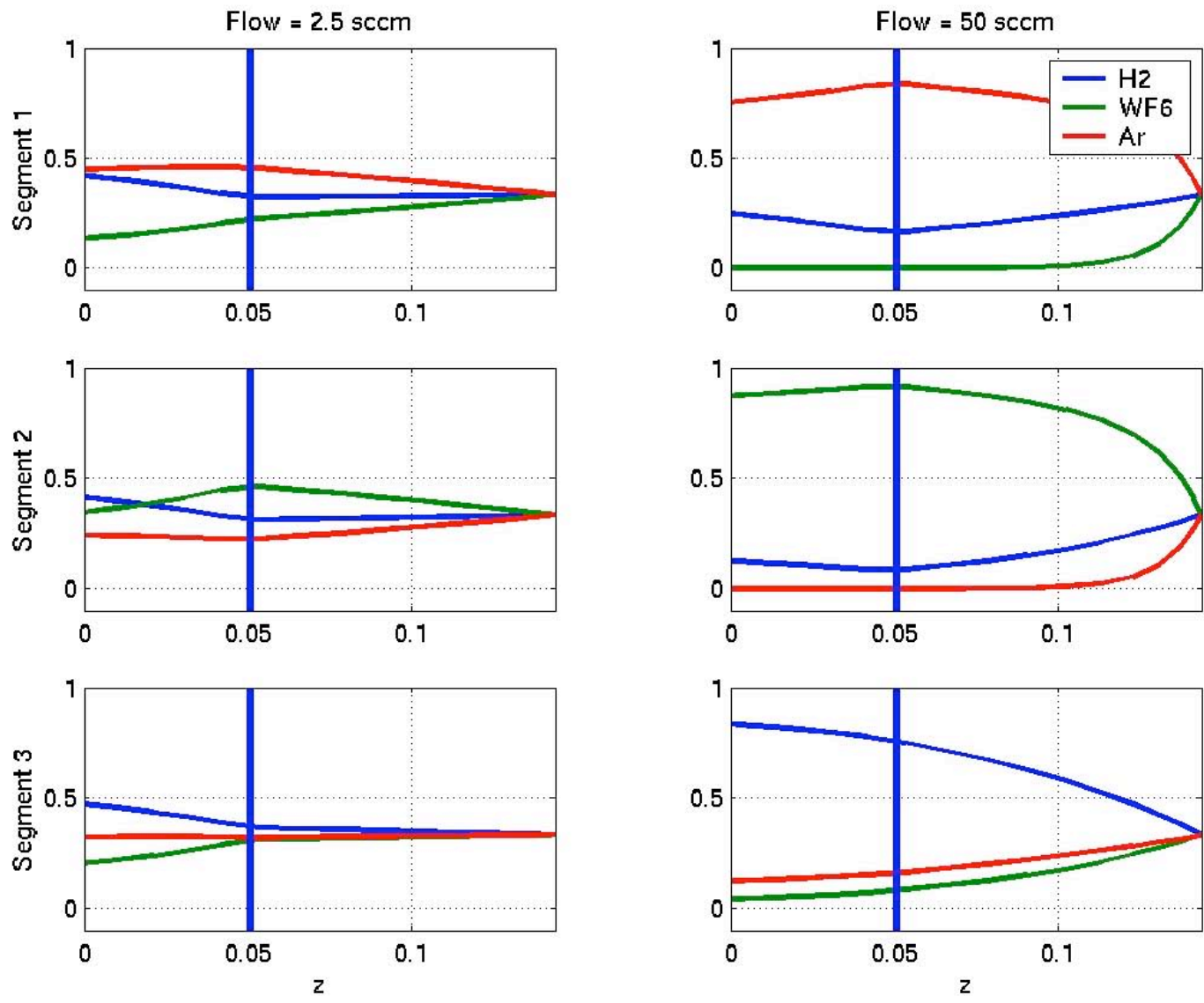


Figure 10

w091202-04

Dep time: 11.3667min

Gap: 1mm

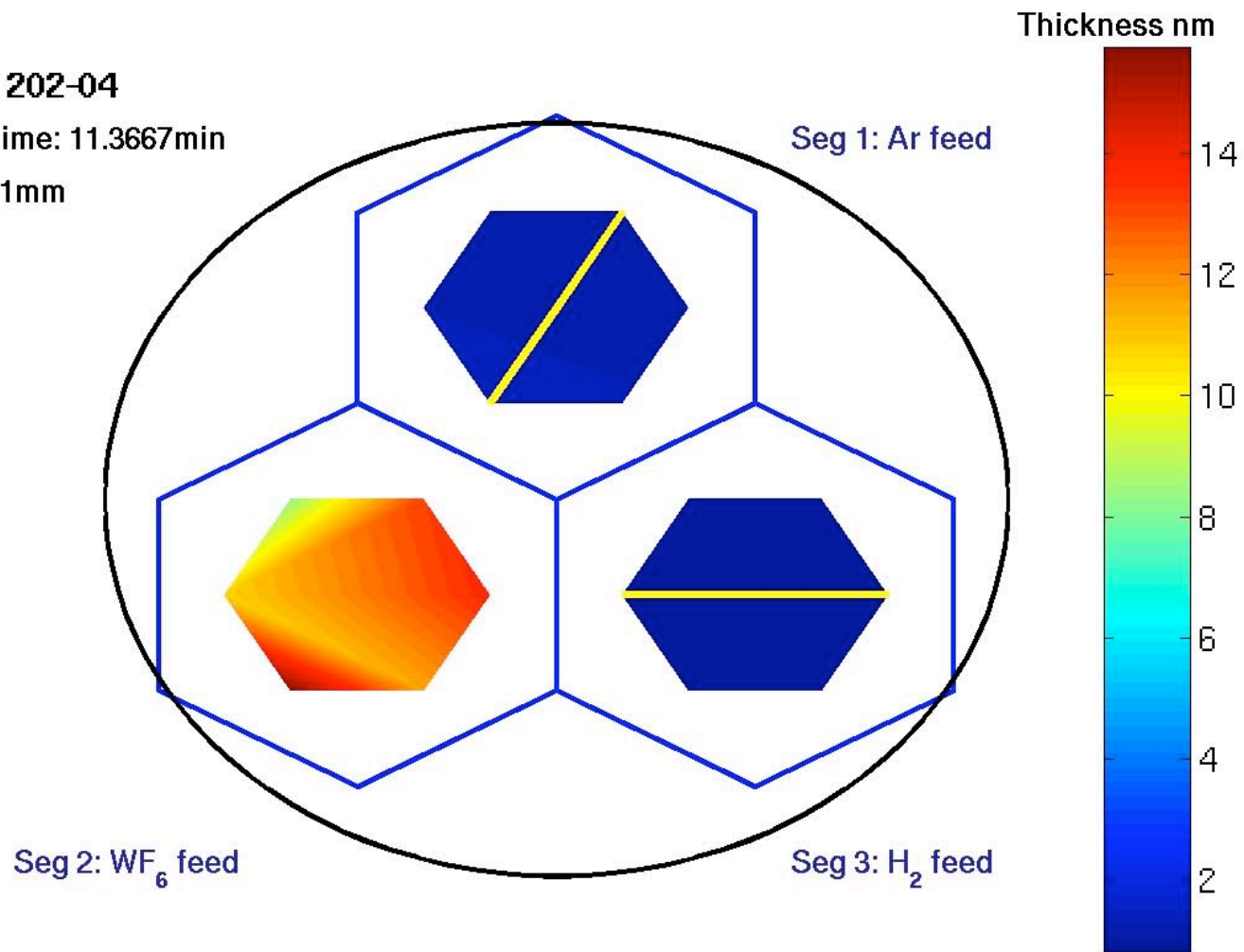
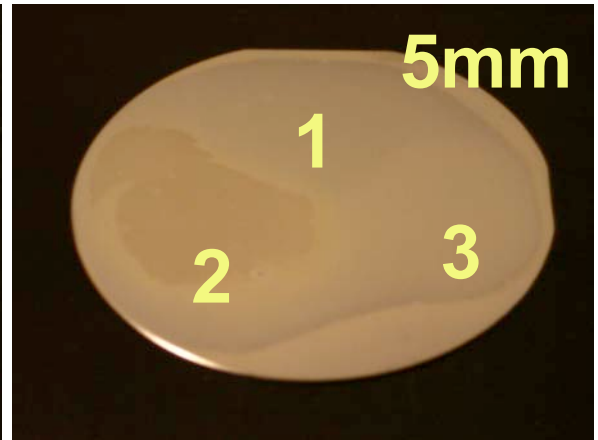
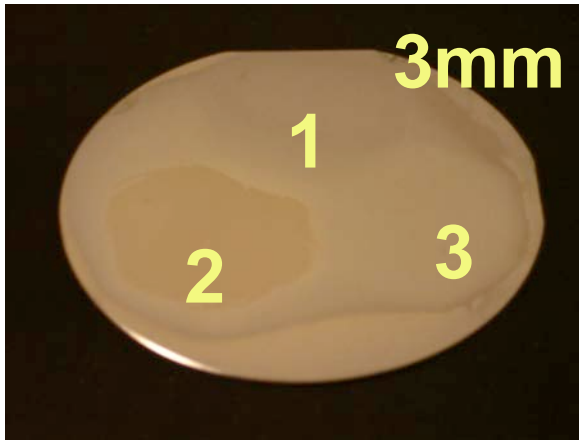
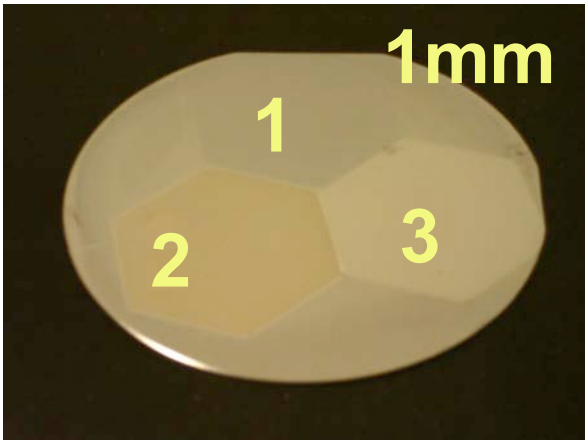
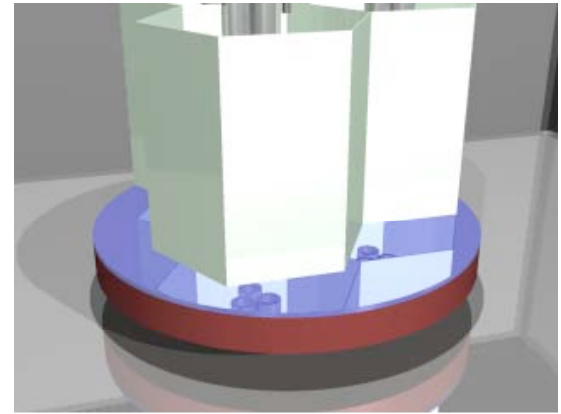
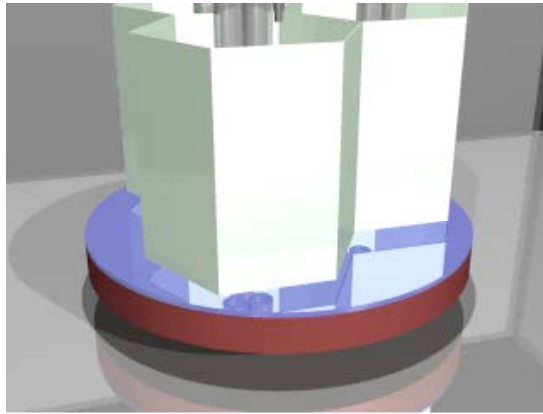
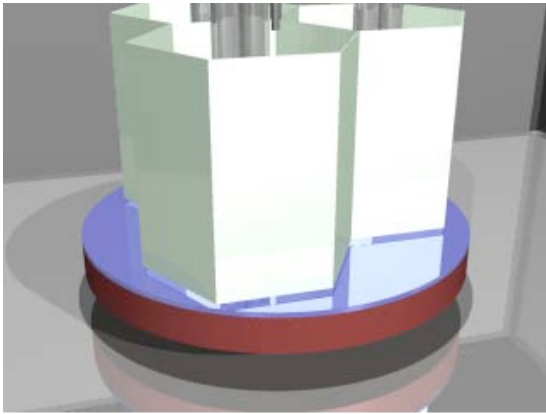


Figure 11



Increasing across-wafer diffusion

Figure 12

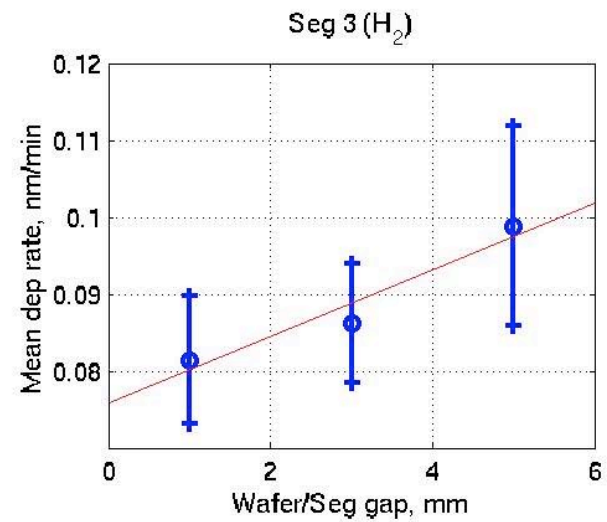
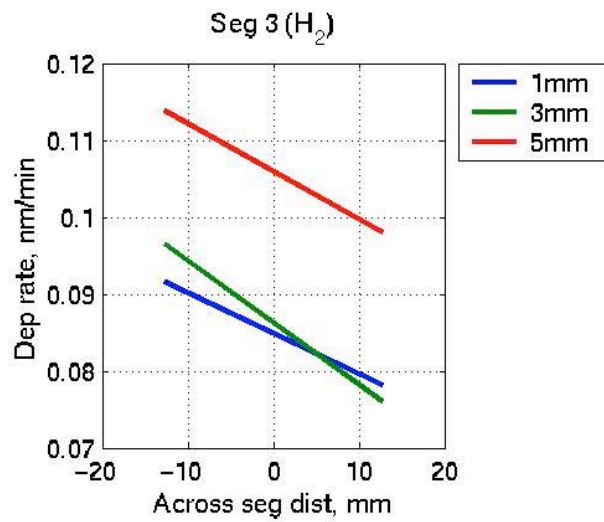
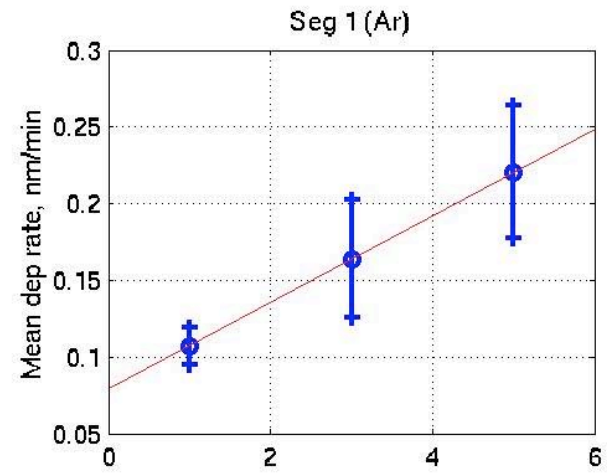
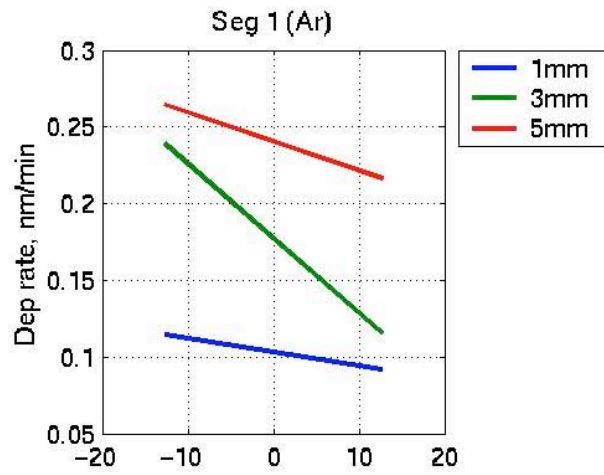


Figure 13

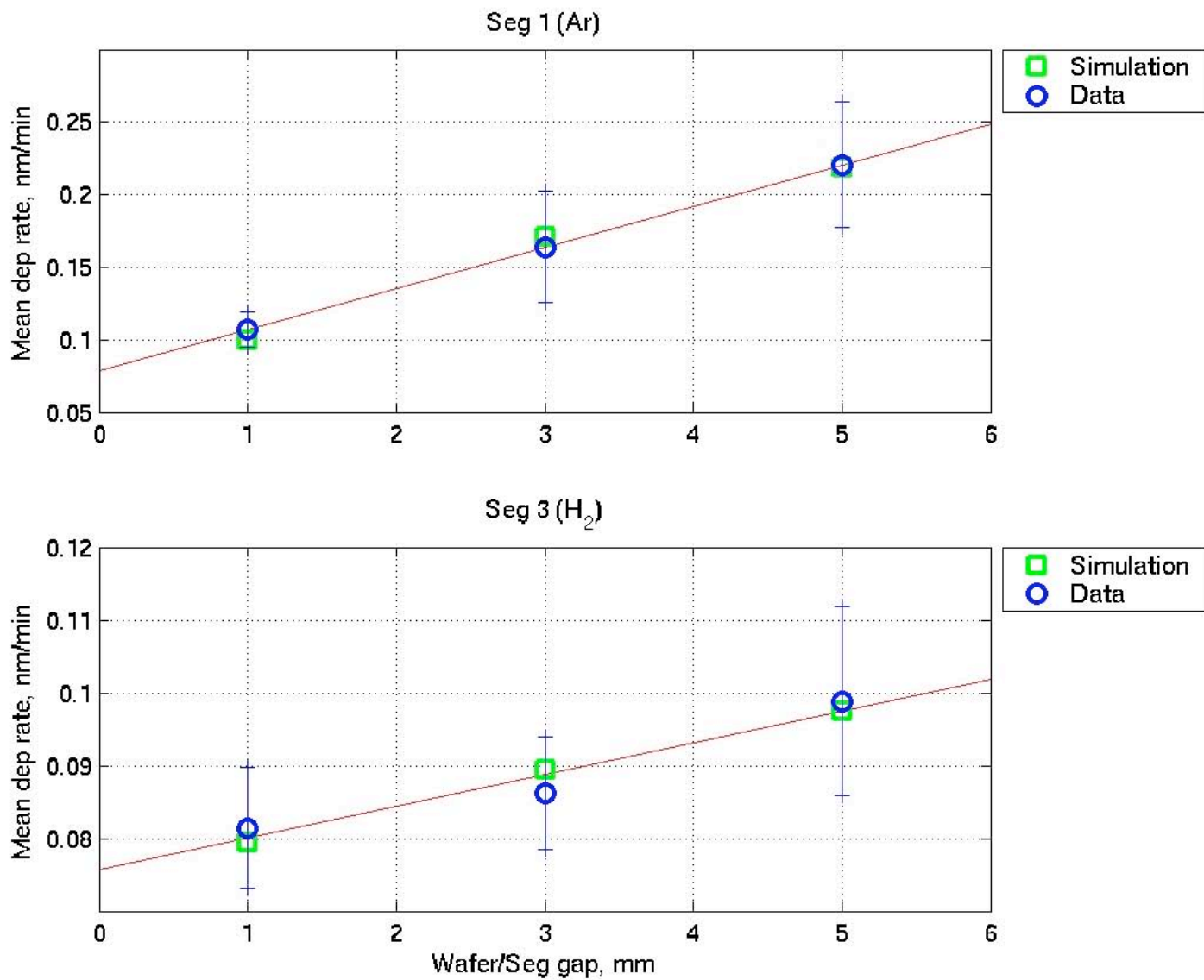


Figure 14